Geochemistry, Geophysics, Geosystems

RESEARCH ARTICLE
10.1029/2018GC008111

Special Section:
Polar region geosystems

Moho Depths of Antarctica: Comparison of Seismic, Gravity, and Isostatic Results

F. Pappa[1], J. Ebbing[1], and F. Ferraccioli[2]

[1]Department of Geosciences, Kiel University, Kiel, Germany, [2]British Antarctic Survey, Cambridge, UK

Key Points:
- Moho depth beneath Antarctica is estimated from inversion of satellite gravity and seismological data
- Results indicate spatially variable buoyancy contribution of the upper mantle in both West and East Antarctica
- Regional 2-D lithospheric modeling demonstrates the need for further seismological constraints in particular in interior East Antarctica

Supporting Information:
- Supporting Information S1

Correspondence to:
F. Pappa,
folker.pappa@ifg.uni-kiel.de

Citation:
Pappa, F., Ebbing, J., & Ferraccioli, F. (2019). Moho depths of Antarctica: Comparison of seismic, gravity, and isostatic results. *Geochemistry, Geophysics, Geosystems*, *20*, 1629–1645. https://doi.org/10.1029/2018GC008111

Received 29 NOV 2018
Accepted 6 MAR 2019
Accepted article online 14 MAR 2019
Published online 28 MAR 2019

Abstract The lithospheric structure of Antarctica is still underexplored. Moho depth estimate studies are in disagreement by more than 10 km in several regions, including, for example, the hinterland of the Transantarctic Mountains. Taking account the sparseness of seismological stations and the nonuniqueness of potential field methods, inversions of Moho depth are performed here based on satellite gravity data in combination with currently available seismically constrained Moho depth estimates. Our results confirm that a lower density contrast at the Moho is present under East Antarctica than beneath West Antarctica. A comparison between the Moho depth derived from our inversion and an Airy-isostatic Moho model also reveals a spatially variable buoyancy contribution from the lithospheric mantle beneath contrasting sectors of East Antarctica. Finally, to test the plausibility of different Moho depths scenarios for the Transantarctic Mountains-Wilkes Subglacial Basin system, we present 2-D lithospheric models along the Trans-Antarctic Mountain Seismic Experiment/Gamburtsev Mountain Seismic experiment seismic profile. Our models show that if a moderately depleted lithospheric mantle of inferred Proterozoic age underlies the region, then a shallower Moho is more likely beneath the Wilkes Subglacial Basin. If however, refertilization processes occurred in the upper mantle, for example, in response to Ross-age subduction, then a deeper Moho scenario is preferred. We conclude that 3-D lithospheric modeling, coupled with the availability of new seismic information in the hinterland of the Transantarctic Mountains, is required to help resolve this controversy, thereby also reducing the ambiguities in geothermal heat flux estimation beneath this key part of the East Antarctic Ice Sheet.

Plain Language Summary Antarctica is a vast and remote continent that is mostly buried beneath the largest ice sheets left on Earth. Consequently, its deep structure is still poorly known, despite its importance as the cradle on which the overlying ice sheets flow. By studying anomalies in the gravitational field of the Earth as measured by satellites and using independent constraints derived by measuring seismic wave travel times from distant earthquakes, we investigate the variations in the depth of the boundary between Earth's crust and mantle (known as the Moho) beneath Antarctica. Our models confirm that the older cratonic regions of East Antarctica have generally deeper Moho compared to the younger geological provinces of West Antarctica. They also highlight that large regions of East Antarctica may exhibit contrasting mantle characteristics, and this lends further weight to recent geological and geophysical studies, indicating that East Antarctica is composed of different Precambrian provinces. In our study we re-evaluated in particular two Moho depth scenarios derived from previous seismic studies for the hinterland of the Transantarctic Mountains, where the enigmatic Wilkes Subglacial Basin lies. We show that if an old Precambrian mantle is assumed, then a thin crust scenario beneath the basin is more likely, but if the mantle has been in part modified by more recent (ca. 500 Ma old) subduction, then a thicker crust scenario would become more viable. Overall, our study calls for combining gravity, seismological, and petrological modeling for enhanced Antarctic lithosphere and isostatic studies.

1. Introduction

The lithosphere of the Antarctic continent is still poorly known, despite several major airborne geophysical campaigns including the acquisition of extensive gravity and magnetic measurements and recent continental-scale data compilations (e.g., Aitken et al., 2014, Aitken et al., 2016; Chiappini et al., 2002; Ferraccioli, Armadillo, Jordan, et al., 2009, Ferraccioli, Armadillo, Zunino, et al., 2009, Ferraccioli et al., 2011; Scheinert et al., 2016; Golynsky et al., 2006, 2018) and a variety of recent seismological studies (e.g.,

An et al., 2015a; Chaput et al., 2014; Hansen et al., 2014; Ramirez et al., 2016; Ramirez et al., 2017; Shen et al., 2017; Shen et al., 2018).

In the last two decades, several Antarctic seismological campaigns have been carried out, in particular within the Fourth International Polar Year (2007–2008). These led to a more robust and comprehensive insight of the crustal thickness and upper mantle structure of Antarctica, and their results have been incorporated in continental-scale Moho depth models. Still, seismological investigations suffer from limited station coverage over large areas. This can lead to large discrepancies in estimates of Moho depth or upper mantle velocities. For example, differences in Moho depth estimation can add up to 10 km, even for the same station (see the supporting information of An et al., 2015a). These differences affect other fields of Antarctic research. Glacial isostatic adjustment studies, for instance, require reliable and robust lithospheric models. Ice sheet dynamics is strongly related to basal melting and geothermal heat flow, which in turn is influenced by crustal thickness variations. It is therefore necessary to attempt to reconcile the different existing data sets by the use of additional geophysical information.

Satellite data are particularly well suited to overcome the remoteness of the Antarctic continent, as they have an almost global uniform coverage (Ebbing et al., 2018). In contrast to surface and airborne surveys, satellite measurements also contain consistent long-wavelength (>150 km) information, which is mainly influenced by deep subsurface structures (Sebera et al., 2018). They are furthermore less affected by near-surface density changes, which are associated with intracrustal geological features. However, potential field methods like gravity suffer inherently from nonuniqueness and thus need additional constraints. In relation to crustal thickness, this can be a certain density contrast at the Moho, in combination with a reference depth, and/or certain depth constraints, for example, from seismology.

Using gravity data, Block et al. (2009) inverted Antarctica's crustal thickness from gravity data by application of the Parker-Oldenberg technique and found Moho depths of ~45 km beneath the southern Transantarctic Mountains (TAM) and the Gamburtsev Subglacial Mountains (GSM). However, seismological studies estimate crustal thickness values of 35–40 km beneath the TAM (Ramirez et al., 2017) and up to 58 km beneath the GSM (Hansen et al., 2010; Heeszel et al., 2013; Ramirez et al., 2016). Considering different values for the density contrast at the Moho, O'Donnell and Nyblade (2014) inverted the crustal thickness of East Antarctica (EANT) and West Antarctica (WANT) with Parker-Oldenberg algorithms separately and used seismic inferred depth values to constrain their results. Their depth values are closer to those from seismological studies but still differ significantly in some regions, for example, the southern TAM. Furthermore, O'Donnell and Nyblade (2014) examined the correlation between the topography and the inverted crustal thickness and recognized missing buoyancy support from the crust for the GSM and Dronning Maud Land in terms of isostatic balance. They suggest alternative mechanisms, such as anomalous middle-to-lower mantle structures, as plausible explanations that could affect the isostatic balance in these regions.

In our study, we invert the depth of the Antarctic Moho with satellite gravity data from the GOCO05s model by using the tesseroid method from Uieda and Barbosa (2017), constrained by seismic depth estimates. Second, we compare our new inversion results with existing seismological Moho depth models and an Airy-isostatic Moho model. High discrepancies are found in some regions, and we discuss these in terms of the potential for different modes of isostatic compensation and upper mantle composition variations beneath different parts of EANT. Specifically, we focus on evaluating two markedly different seismologically derived Moho depth estimations in the hinterland of the TAM in the Wilkes Subglacial Basin region, along the Trans-Antarctic Mountain Seismic Experiment (TAMSEIS)-GAmburtsev Mountain SEISmic experiment (GAMSEIS) profile (Hansen et al., 2009; Lawrence et al., 2006a, 2006b) by using 2-D models of the lithosphere and the sublithospheric upper mantle. These models incorporate isostasy, the thermal field, seismic velocities, mantle petrology, geoid, and heat flow estimations. Using this approach, we demonstrate that both thinner and thicker crusts beneath the Wilkes Subglacial Basin can lead to an acceptable fit of the observed satellite gravity data. However, we also show that the thinner-crust scenario is preferred if the region is underlain by a moderately depleted lithospheric mantle of inferred Proterozoic age, while the thicker crust is more likely if refertilization processes likely linked to Ross-age (ca. 500 Ma) subduction (e.g., Ferraccioli et al., 2002) along the margin of the composite East Antarctic craton are invoked. Overall, we conclude that satellite gravity data can complement seismological observations thereby providing an important tool for the development of new 2-D and 3-D models of the Antarctic crust and deeper lithosphere.

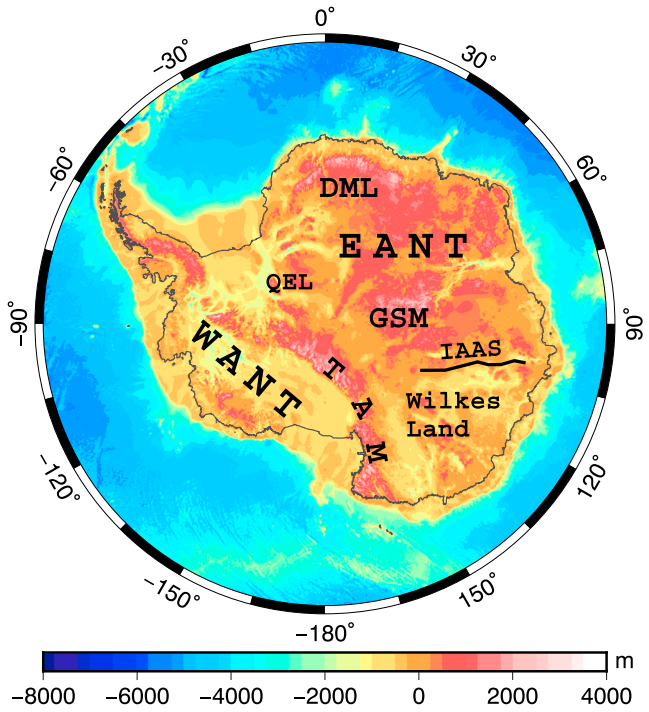

Figure 1. Bedrock topography of Antarctica from Bedmap2 model (Fretwell et al., 2013). WANT = West Antarctica; EANT = East Antarctica; DML = Dronning Maud Land; GSM = Gamburtsev Subglacial Mountains; IAAS = Indo-Australo-Antarctic Suture; QEL = Queen Elizabeth Land; TAM = Transantarctic Mountains.

2. Data

2.1. Bedrock Topography and Gravity Data

Bedmap2 is a compilation of the ice thickness and the bedrock topography (Figure 1) of Antarctica up to latitude 60°S and is mainly based on airborne radar surveys (Fretwell et al., 2013). Even though some areas are not well covered and exhibit large uncertainties of up to >1,000 m, it is the best ice thickness model currently available for Antarctica. The data set is provided as an interpolated grid with 1-km spacing.

We use the combined gravity model GOCO05s (Mayer-Guerr, 2015) to obtain the geoid undulation and the vertical gravity over Antarctica (Figure 2). In order to suppress contributions in the signal from below the lithosphere, the geoid is calculated in spherical harmonics from degree and order 12 up to 280 (maximum of the GOCO05s model). The truncation of $N < 12$ is commonly done to eliminate long-wavelength components from the signal, which are associated with sublithospheric sources (Fullea et al., 2009, and references therein). The geoid is in particular used in the 2-D modeling (ch. 4).

Second, we take the gravity disturbance signal (Figure 2) at a height of 50 km from the GOCO05s model. The gravity disturbance is a form of free air anomaly reduced to the surface of the normal Earth ellipsoid (Li & Götze, 2001). The representation of the field at 50 km is chosen, as it offers a higher level of detail in the signal than at satellite altitude (~250–500 km) and ensures that the noise amplification is still acceptable for the purposed of crustal thickness and lithospheric modeling (e.g. Sebera et al., 2014).

The total gravity signal originates from several sources, and the free-air anomaly is largely affected by topography and its isostatic compensation. However, we are interested in the Moho geometry and therefore compute the Bouguer gravity anomaly, where the signal arising from the bedrock topography and ice thickness variations is corrected for. In the Bouguer anomaly, the density contrast at the crust-mantle boundary in most cases has a dominating influence on the gravity signal. Even though the remaining signal possibly still contains effects from density variations within the crust or the mantle, or an imperfect topographic reduction model, the Bouguer anomaly can be regarded as suitable for an inversion of the Moho geometry. To compute the Bouguer anomaly above Antarctica, we use density values for water ($\rho_{water} = 1{,}028$ kg/m^3), ice ($\rho_{ice} = 917$ kg/m^3), and bedrock elevation ($\rho_{topo} = 2{,}670$ kg/m^3) together with the ice thickness and topography information from Bedmap2. In our gravity data processing, we also account for far-field and edge effects from masses outside the model area. Szwillus et al. (2016) demonstrated that both topographic masses and isostatic effects need to be considered in a global background model for continental-scale areas of interest. We use the ETOPO1 (Amante & Eakins, 2009) data set to compute a global topographic correction model and a simple Airy-isostatic Moho model ($z_{ref} = 30$ km, $\Delta\rho = 450$ kg/m^3). For both models, Antarctica is cut out because we have the better topographic model from Bedmap2, and the Moho is to be inverted for the continent. The result is a Bouguer gravity anomaly above Antarctica (Figure 3), which most closely corresponds to the signal from the crust-mantle boundary.

2.2. Seismological Models

We make use of previous seismological studies in two ways. First, we use points of seismic Moho depth estimates to constrain our gravity inversion and thereby attempt to overcome the inherent ambiguity of potential field methods. Second, we evaluate existing continent-wide Moho depth models based on seismology in terms of their gravity signal and compare them with our inversion results. Thus, a set of points with Moho depth estimations as well as a gridded Moho depth model is needed for our purpose. In this study we revert to the models (a) "AN1-Moho" from An et al. (2015a), which is a 3-D *S* wave velocity model resulting from Rayleigh wave dispersion analyses, and (b) "ANT-Moho" from Baranov and Morelli (2013), which is a

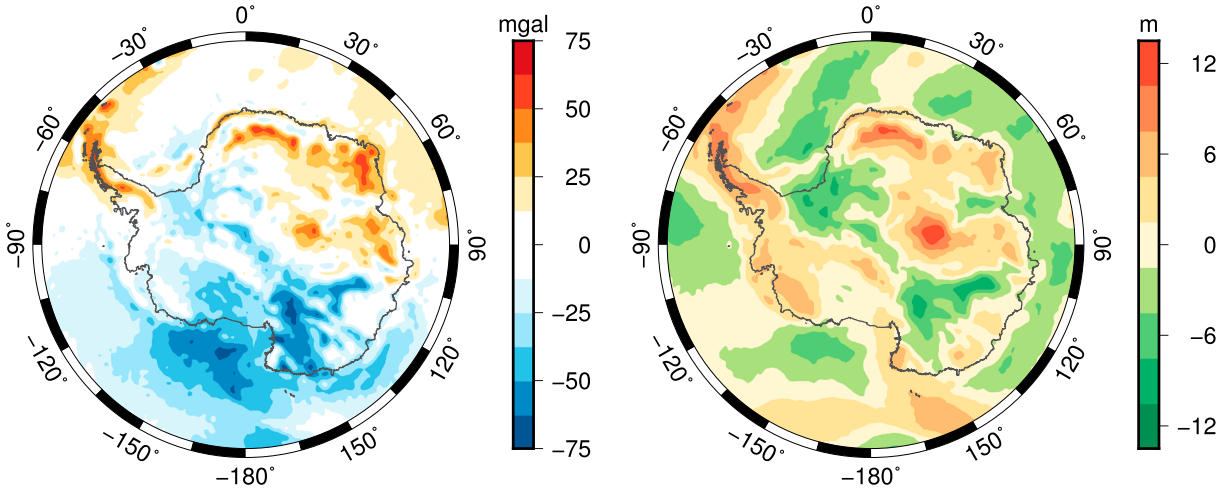

Figure 2. Gravity disturbance at 50-km altitude (left) and geoid (right) from GOCO05s model. The geoid is computed from spherical harmonics expansion from degree and order $N = 12$ to 280.

compilation of regional seismological surveys, interpolated with the standard kriging method (Figure 4). More recent studies exist (e.g., Ramirez et al., 2016; Ramirez et al., 2017; Shen et al., 2018, 2017) but do not cover whole Antarctica or do not provide both single points and areal Moho depth estimation.

Although the AN1-Moho and the ANT-Moho reflect the strong contrast in crustal thickness between WANT (~25 km) and EANT (~40 km), they disagree in large parts and differ up to 20 km in depth (Figure 4). In particular, the crustal thickness of Wilkes Land (compare Figure 1) is estimated to be ~40 km in the AN1 model, while the ANT model shows values of ~30 km. Not only do the two seismological models exhibit wide disparities in many regions of Antarctica but they also contradict the observed gravity signal when a certain density contrast at the Moho is assumed. Figure 4 shows the mismatch of both models against the Bouguer

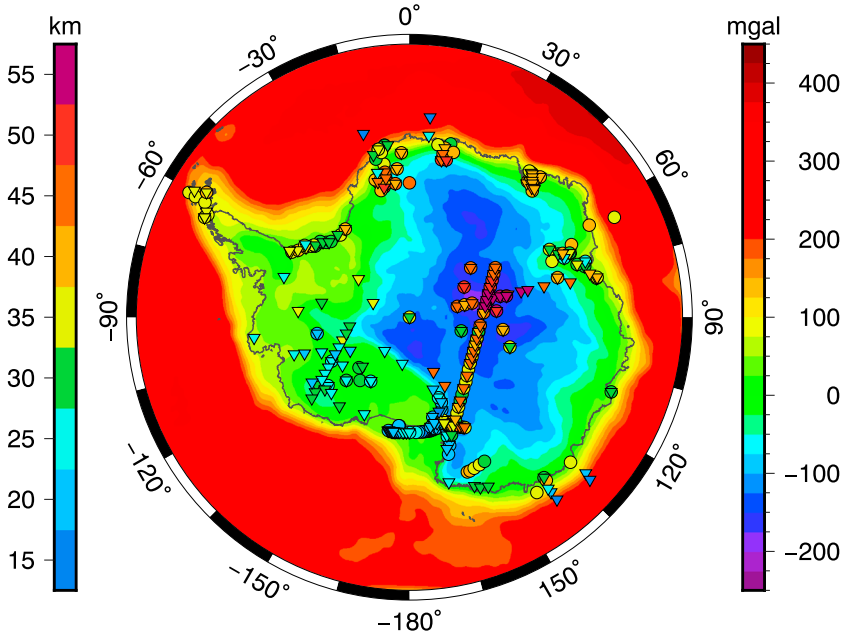

Figure 3. Bouguer gravity anomaly above Antarctica used as input for the Moho depth inversion. Gravity data from GOCO05s in 50 km height corrected for effects from ice, water, and bedrock topography. In addition, the effect from a global Airy-isostatic Moho outside the model area is subtracted. The point sets of seismologically constrained Moho depth values are represented by colored triangles (AN1 model) and circles (ANT model).

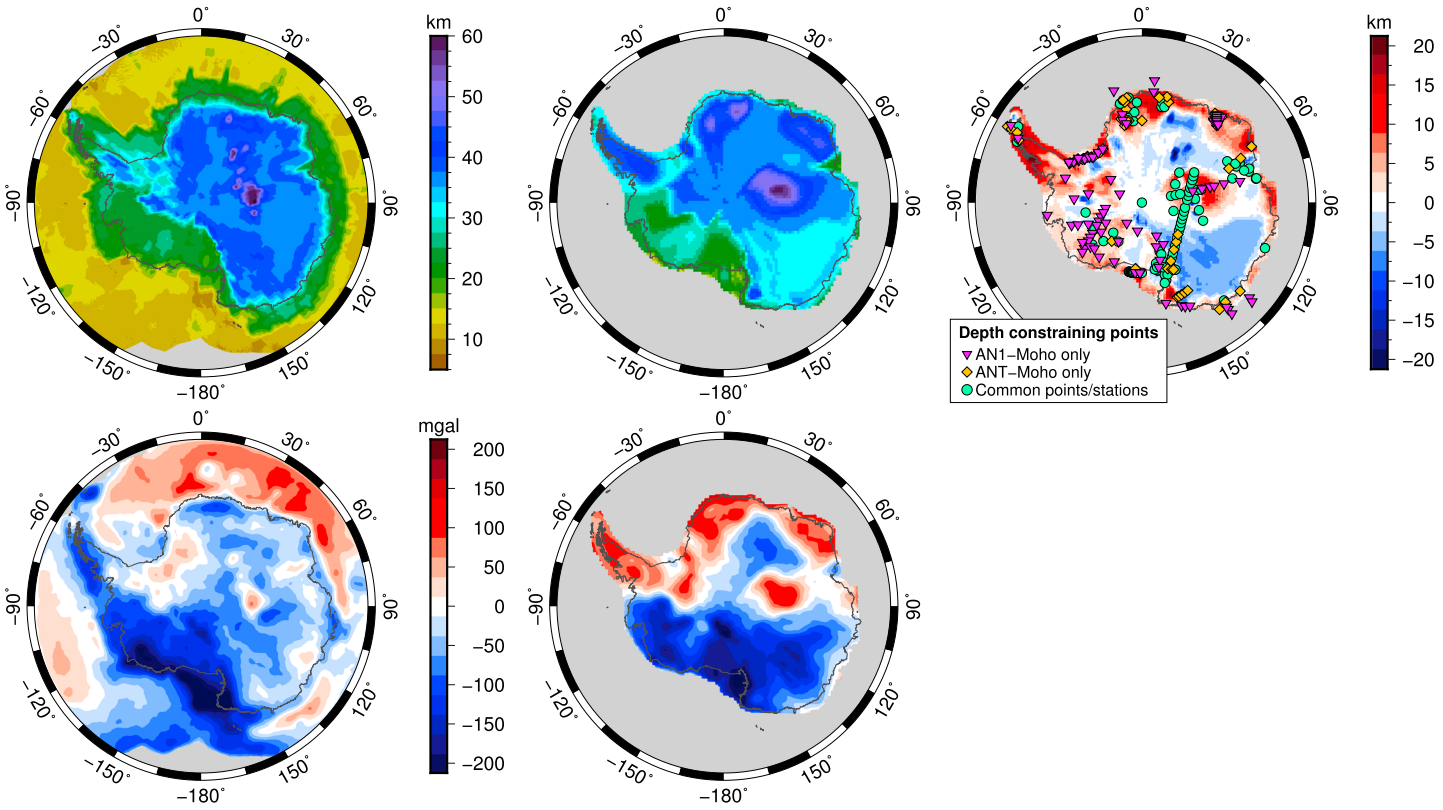

Figure 4. Top: Depth maps of seismic Moho depth models. Left: "AN1-Moho" is derived from an *S* wave velocity model based on Rayleigh wave dispersion analyses (An et al., 2015a); center: "ANT-Moho" is a compilation of regional surveys (Baranov & Morelli, 2013). The strongest differences (right figure) between both models occur in the Wilkes Land, Dronning Maud Land, the periphery of the Gamburtsev Subglacial Mountains, and the Antarctic Peninsula. Bottom: Misfit of forward-calculated gravity effects from seismological Moho depth models (left: AN1; right: ANT) compared to satellite-inferred gravity data at 50 km height. Both models show large disagreement with the gravity data and between each other.

gravity anomaly after forward computation of their gravity signal. This disagreement is independent from the applied Moho reference depth and density contrast. Merely, the amplitude of the misfit varies. Considering the calculated Bouguer anomaly to be correct, this implies that either the density contrast at the Moho varies strongly across Antarctica or the seismological models do not represent the actual Moho depth, or a combination of these factors.

Both models are constrained by a set of seismic station points from other studies (see An et al., 2015a; Baranov & Morelli, 2013, and references therein), where the Moho depth is regarded as well constrained (Figure 3). Yet, even though many stations are included in both the ANT and the AN1 model, they indicate different Moho depth values, depending on the applied seismological method. This certainly had an influence on the discrepancy between the final models. We take these point sets as a benchmark for the Moho depth models in the gravity inversion. The points from the AN1 and the ANT model will first be used separately, and additionally in combined set to evaluate the gravity-inverted Moho depth models.

3. Moho Depth Inversion From Gravity

3.1. Methodology

We follow the methodology of Uieda and Barbosa (2017), who applied a nonlinear inversion algorithm on gravity and seismic data for South America with the Python code package Fatiando. A tesseroid model is created to reproduce the preprocessed gravity signal, parametrized by (1) a regularization parameter, which controls the smoothness of the model; (2) the reference depth (normal Earth Moho depth: z_{ref}); and (3) the density contrast $\Delta\rho$ at the Moho. The regularization parameter is estimated by the inversion of multiple test sets, derived from the original data set. The parameter value that results in the least mean square error

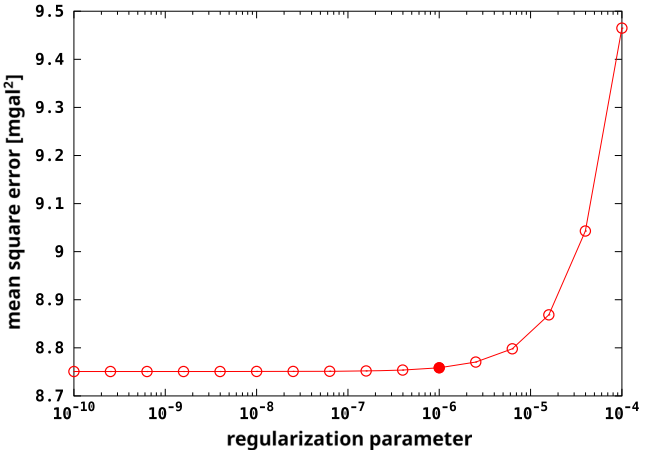

Figure 5. Cross-validation curve of the regularization parameter. No local minimum exists. The value of 10^{-6} is chosen since lower values do not lead to a significantly lower mean square error.

(MSE) in predicting the original data set is taken to be optimal. However, we did not find a local minimum within our interval of values for the regularization parameter (10^{-10} ... 10^{-4}). We therefore chose the value of 10^{-6} from which on no further improvement in the MSE can be observed (Figure 5).

The two other parameters z_{ref} and $\Delta\rho$ span a parameter space for given intervals. Since the mean depth of the Moho and its density contrast are poorly known for Antarctica, we set a wide range for both parameters: The reference depth in 2.5 km steps from 25 to 40 km, and the density contrast in 25 kg/m^3 steps from 250 to 550 kg/m^3. For each pair of reference depth and density contrast in this discretized parameter space, the inversion is performed with the previously estimated regularization parameter. Afterward, the results are evaluated against a set of points with verified Moho depth values from seismic experiments. Finally, the model that gives the smallest MSE in this evaluation is taken as the best fitting one. Further details of the methodology are described by Uieda and Barbosa (2017).

Since the Fatiando Python code demands an equiangularly discretized gravity data set to create a similarly discretized tesseroid model, all data sets used for the inversion are relocated from the South Pole to the equator. The geographical coordinates from the Antarctic environment are projected into Cartesian coordinates with a Lambert Equal Area projection and subsequently reprojected into geographical coordinates at the equatorial region from 30°W to 30°E and 30°S to 30°N. This is done with a spherical Earth in order to avoid distortions due to the use of the WGS84 ellipsoid.

We perform three separate inversions for individual sets of seismological Moho depth points: at first for the point set that was used by An et al. (2015a) to constrain their Moho depth model ("AN1"), second for the point set used for the kriging-interpolated compilation from Baranov and Morelli (2013) ("ANT"), and third a combined set of both ("comb"). Additionally, we aim to address the different tectonic settings of WANT and EANT in separate inversions, using only seismic points inside the respective area.

3.2. Inversion Results

Depending on the point set of seismological Moho depth values, different pairs of reference depth and density contrast yield the best fit (Figure 6). While the least error for the "AN1" set is found at $z_{ref} = 27.5$ km and $\Delta\rho = 350$ kg/m^3, the "ANT" set is best fitted with $z_{ref} = 30$ km and $\Delta\rho = 450$ kg/m^3. The optimum of the combined set is at $z_{ref} = 30$ km and $\Delta\rho = 425$ kg/m^3. Consequently, the inverted Moho depths differ. The maximum depth of all models is about 45 km, consistent with the gravity inversion results from Block et al. (2009), and they overall agree in EANT. In WANT, however, the model inverted with the point set "AN1" shows a 3- to 5-km shallower Moho than the other two, which comes along with the lower density contrast.

As O'Donnell and Nyblade (2014) emphasize, a single inversion for the whole continent with one constant density contrast and Moho reference depth results in a compromise between the distinct blocks of cratonic EANT and rift-dominated WANT. We too see this effect very apparent in the map images and the mismatch histograms in Figure 6. The latter show two distinct Gaussian curves, reflecting the western and the eastern part of Antarctica. Thus, we also conducted the inversion procedure with seismic points from the combined set constrained to the respective area of WANT and EANT (Figure 7). For WANT we find a well-resolved optimal reference depth of ~25 km. The density contrast, however, is rather diffuse without a clear optimum. We interpret this as an indication of a strong heterogeneity in the region. Compared with this, we also find a distinct reference depth for EANT at $z_{ref} = 35$ km but also a better resolved optimal density contrast of $\Delta\rho = 625$ kg/m^3. In this particular case, the reference depth seems reasonable and corresponds to the cratonic nature of EANT. However, the density contrast is most likely overestimated, since the gravity signal needs to be reproduced over the whole study area, including WANT and oceanic areas. Regardless of this, the derived Moho topography beneath EANT reflects the best fit according to the seismic depth points inside the area. In both parts of Antarctica, the misfit concerning the seismic depth points is decreased significantly

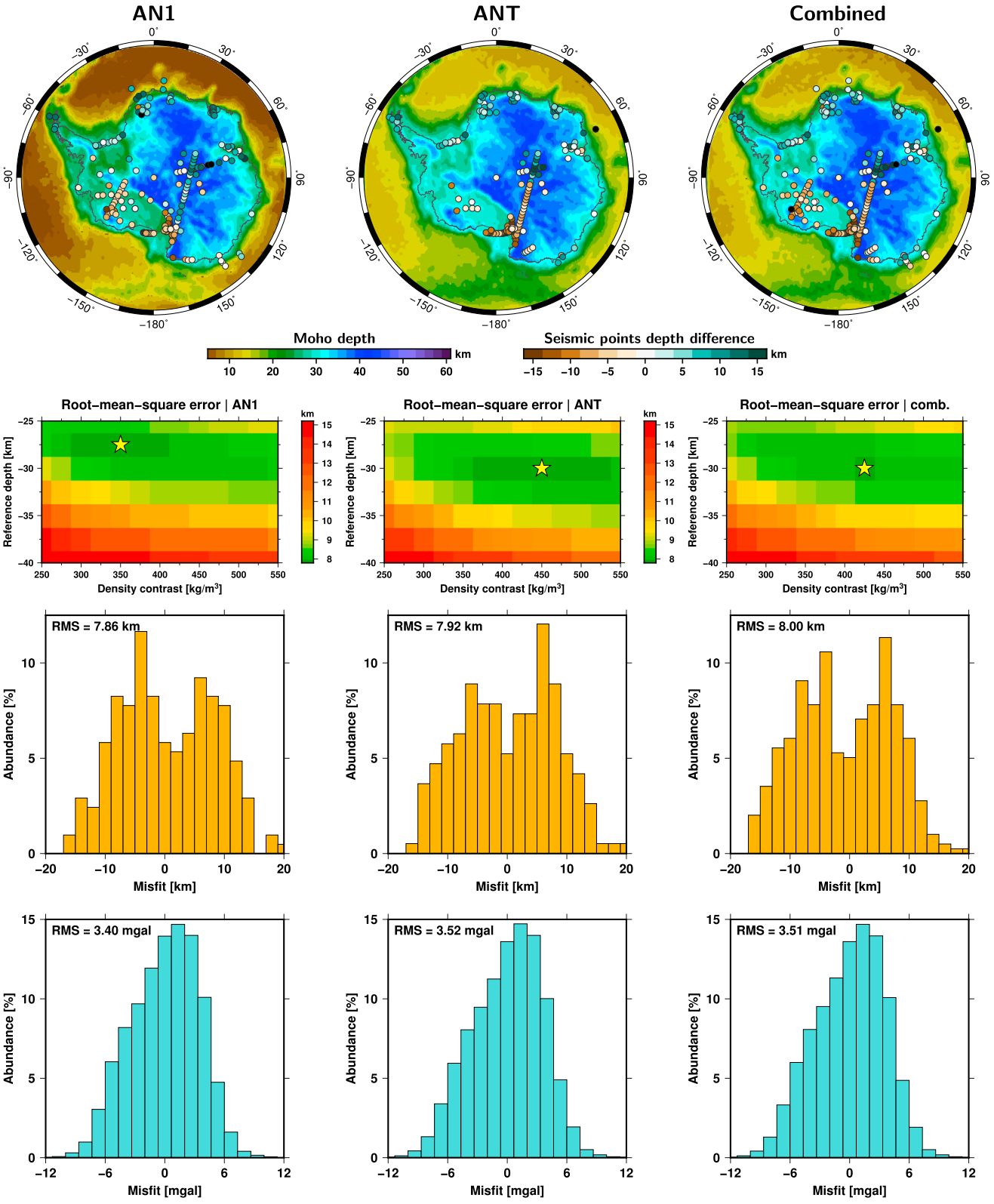

Figure 6. Top: Resulting Moho depth maps from the inversion for different seismic depth point sets (from left to right: AN1, ANT, and combined). The colored circles indicate the differences in depth between the seismic constraint and the inverted depth. Second row: root mean square (RMS) error within the applied parameter space. The best fitting pair of reference depth and density contrast is marked by the star symbol. Underneath: histograms of Moho depth difference and corresponding RMS. Bottom: histograms of gravity residuals.

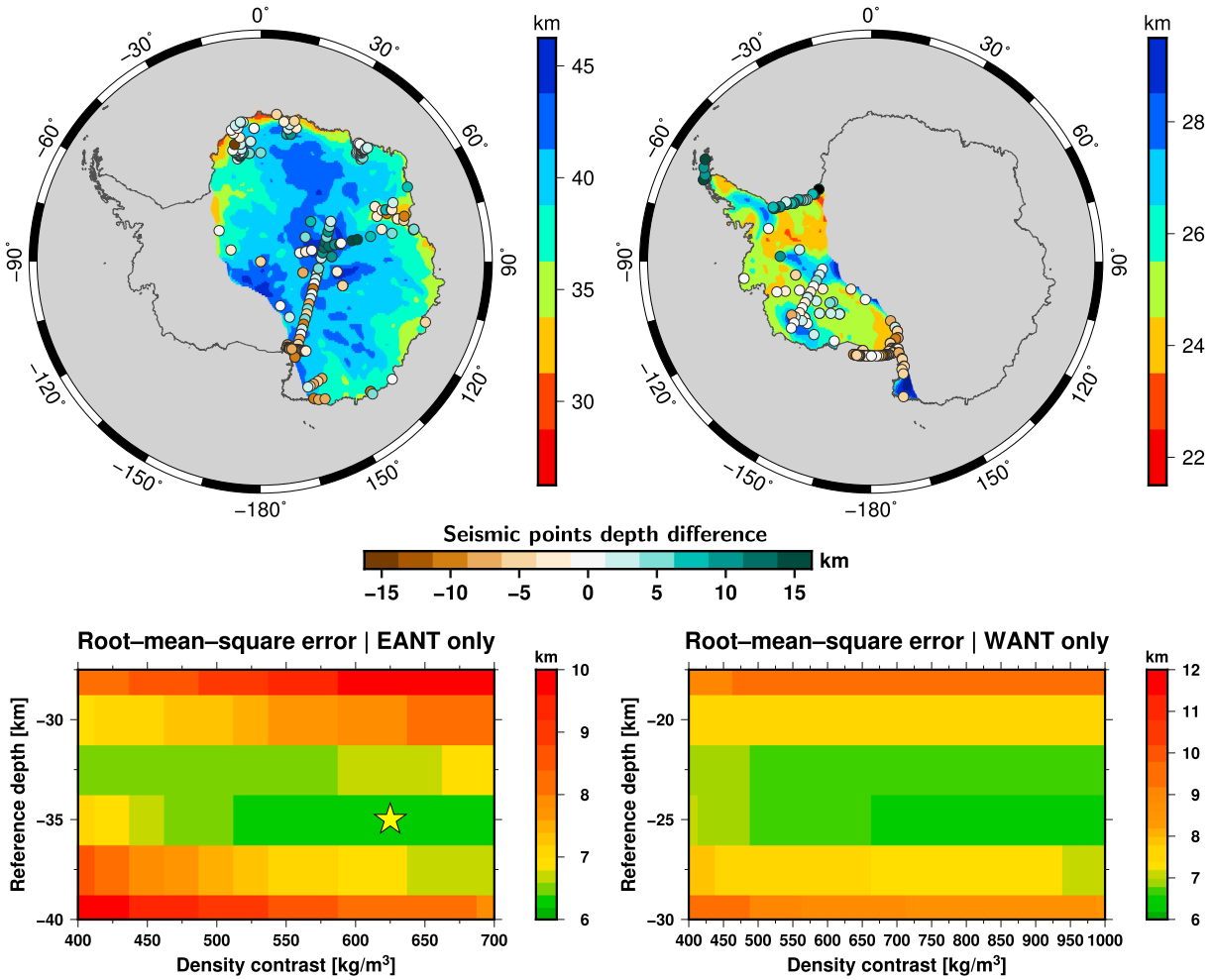

Figure 7. Top: resulting Moho depth maps from the inversion with separate seismic points for EANT (left) and WANT (right). The colored circles indicate the differences in depth between the seismic estimate and the inverted depth. Bottom: root mean square error of gravity-inverted Moho depth to seismic points. While still a rather clear optimum could be found for EANT at $z_{ref} = 35$ km and $\Delta\rho = 625$ kg/m^3, the inversion for WANT shows only a distinct reference depth of ~25 km. The density contrast, on the other hand, is rather diffuse, which is pointing toward a strong heterogeneity in the area. WANT = West Antarctica; EANT = East Antarctica.

compared to the inversion for the whole continent. Still, the density contrast could not be determined reliably in the separate inversions.

3.3. Comparison With Seismological Moho Depth Models

Although the applied inversion methodology is taking account of the seismic-inferred depth points, the resulting Moho depth model still has to reproduce the gravity data and is not expected to fit the seismic data perfectly. This is reflected in Figure 6 (bottom) by the small mismatch in the gravity signal (RMS ≈ 3.5 mgal) and the relatively high residual in the Moho depth (RMS ≈ 8 km). While in Figure 6 the gravity-inverted Moho depth is compared with the seismic points (indicated by the colored circles), Figure 8 shows the complete depth differences between the gravity inverted and the areal seismological models.

Large parts of EANT are within the typical range of seismological uncertainty in Moho depth estimation (approximately ±4 km). On the other hand, strong differences occur beneath the GSM and in Queen Elizabeth Land (compare Figure 1) for both models. The TAM, in particular their southernmost part, and whole WANT have a much higher crustal thickness in the gravity inverted models than seismic estimations indicate. The same pattern is reflected by the gravity misfit of the original seismological models (Figure 4).

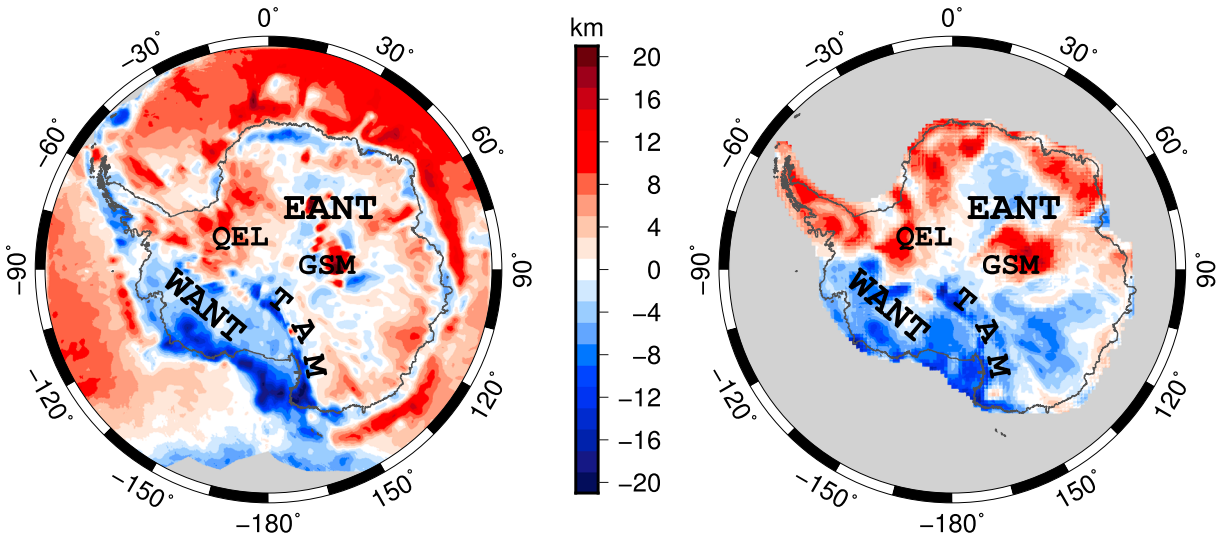

Figure 8. Depth difference between gravity-inverted and seismological Moho depth models (left: AN1; right: ANT). Most parts are within the typical uncertainty range of seismological methods. Both seismological models indicate greater Moho depth beneath QEL and the GSM than the gravity inversion. WANT = West Antarctica; EANT = East Antarctica; GSM = Gamburtsev Subglacial Mountains; QEL = Queen Elizabeth Land; TAM = Transantarctic Mountains.

3.4. Comparison With Isostatic Moho Model

The discrepancies between the seismological Moho depth estimations and the gravity signal raise questions about the mass distributions within the Antarctic lithosphere and its isostatic state. For the purpose of this comparison, we calculate simple Airy-isostatic Moho depth models for the continent, using the same values for reference depth and density contrast as derived from the inversion (Figure 9). The residual map reveals strong deviations from Airy-isostasy when applying a single density contrast at the Moho boundary. These patterns are congruent with those of the gravity disturbance (Figure 2) and the gravity residual resulting from the Airy-isostatic crustal model (Figure 9). Most prominent are the TAM and Wilkes Land, where the gravity inverted Moho depth is up to 10 km deeper than Airy-isostasy is suggesting. The GSM and Dronning Maud Land are almost not visible in the residual map.

However, in both residual maps we can identify a different signature not only for WANT and EANT but also within EANT itself: between the TAM and the proposed Indo-Australo-Antarctic Suture (Aitken et al., 2014), where Indo-Antarctica and Australo-Antarctica may have collided either during the late Mesoproterozoic or as late as the early Cambrian (Boger, 2011; Collins & Pisarevsky, 2005), the residual is substantially lower than for the rest. This may either point at different modes of isostatic compensation

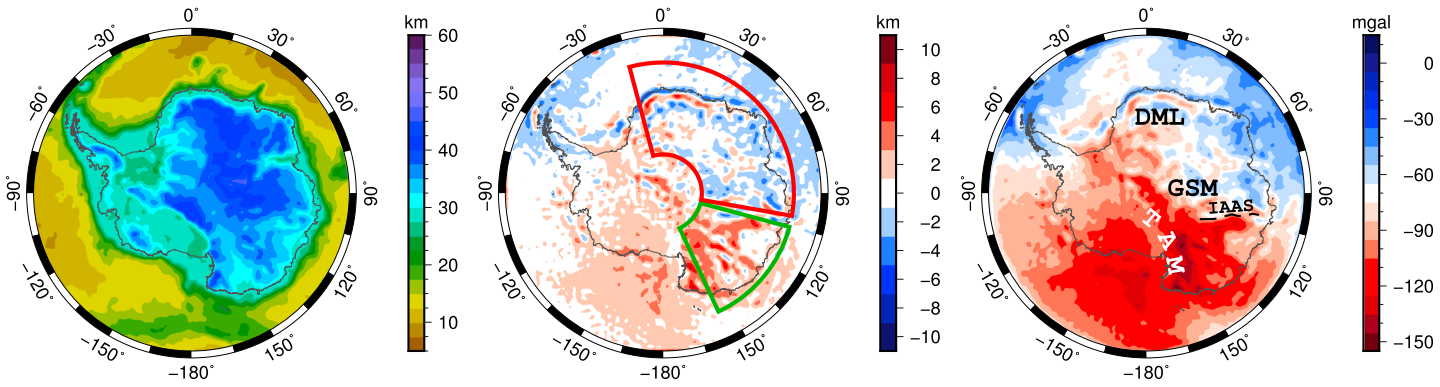

Figure 9. Left: Airy-isostatic Moho depth calculated with density contrast and reference depth from the inversion with combined seismic data point set; center: depth difference between gravity-inverted and Airy-isostatic Moho; right: gravity residual resulting from the Airy-isostatic Moho. IAAS = Indo-Australo-Antarctic Suture; DML = Dronning Maud Land; TAM = Transantarctic Mountains.

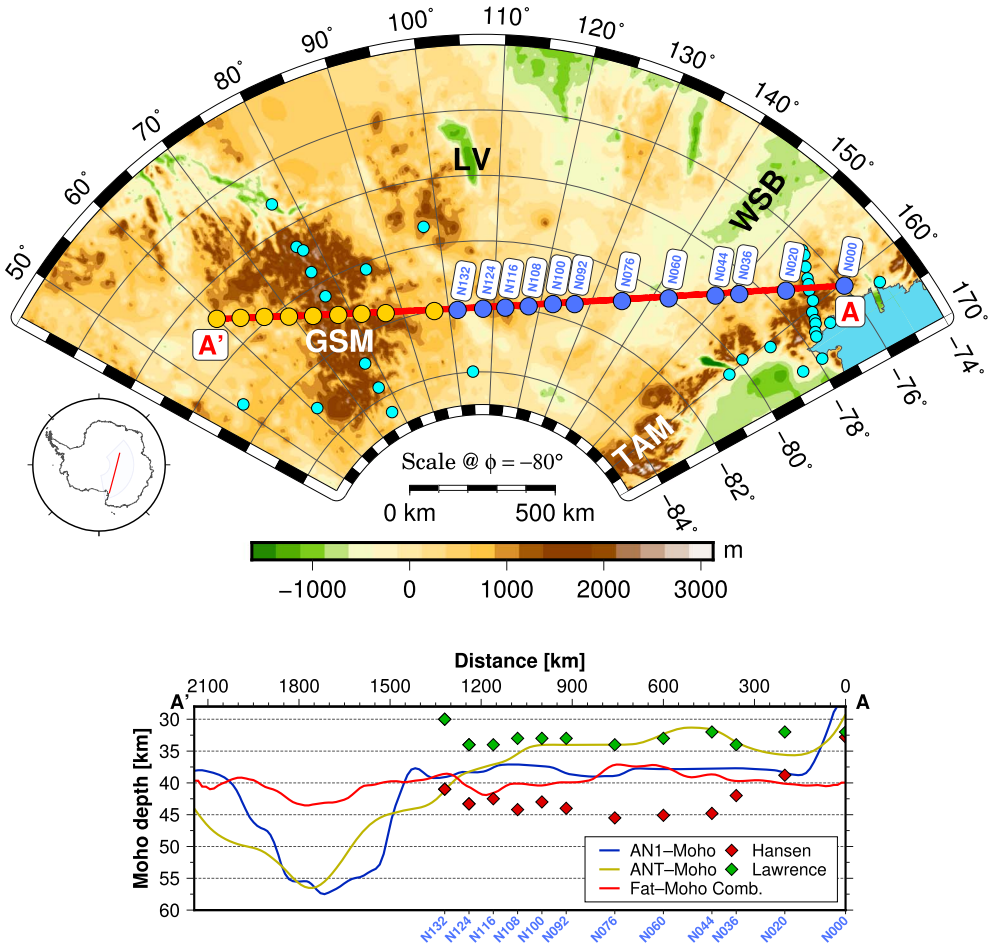

Figure 10. Top: Bedrock topography (Fretwell et al., 2013) with combined profile (A-A′) of seismic stations from the Trans-Antarctic Mountain Seismic Experiment (blue circles) and Gamburtsev Mountain Seismic experiment (orange circles) surveys. Cyan-colored circles indicate further seismic stations used to constrain the AN1-Moho model. GSM = Gamburtsev Subglacial Mountains; LV = Lake Vostok; TAM = Transantarctic Mountains; WSB = Wilkes Subglacial Basin. Bottom: Moho depth estimations from different studies: Rayleigh wave analyses from Lawrence et al. (2006b) show a shallow Moho at ~30 km (green diamonds), while *S* wave receiver functions from Hansen et al. (2009) indicate an ~10-km deeper Moho (red diamonds). Solid lines indicate depth of seismic (AN1-Moho and ANT-Moho) and gravity-inverted Moho with combined point set.

(e.g., lithospheric mantle densities) or imply that topography is partly supported by dynamic (i.e., deeper mantle) effects.

4. 2-D Lithospheric Cross-Sections

Our analysis shows that the mass distribution in the crust and upper mantle is expected to have a significant role in the isostatic state and gravity field of Antarctica. In the following, we discuss the potential upper mantle contribution by 2-D modeling across the Wilkes Subglacial Basin region of EANT in particular.

As mentioned previously, large disagreements exist between different Moho depth models and studies in EANT. Moho depth estimates from seismological studies differ for the same station by up to 10 km, even along a relatively well-studied profile (Figure 10). The profile stretches from the TAM to the GSM (Creyts et al., 2014; Paxman et al., 2016) crossing the southern Wilkes Subglacial Basin (Ferraccioli et al., 2001; Ferraccioli, Armadillo, Jordan, et al., 2009; Ferraccioli & Bozzo, 2003; Jordan et al., 2013; Paxman et al., 2018, 2019; Studinger et al., 2004). Seismic data have been acquired by deployments from the TAMSEIS (Hansen et al., 2009; Lawrence et al., 2006a, 2006b) and the GAMSEIS (Kanao et al., 2014) experiments.

Yet the respective studies are not consistent and yield different Moho depth estimations, ranging from a relatively shallow (~33 km, Rayleigh wave analyses; Lawrence et al., 2006b) to a significantly deeper (~43 km, *S* wave receiver functions; Hansen et al., 2009) Moho beneath the southern Wilkes Subglacial Basin. Similar discrepancies exist between the AN1-Moho model (deep), which incorporates estimates from Hansen et al. (2009), and the ANT-Moho model (shallow), involving results from Lawrence et al. (2006b). Such a considerable difference of ~10 km in crustal thickness has, of course, strong implications for the characteristics of the crust itself and the underlying mantle in terms of density, temperature, and composition and therefore the tectonic and geodynamic history of the region. In case of pure Airy-isostasy, for example, 10 km in crustal thickness would correspond to 1,500 m in topography, when assuming a rock density of 2,670 kg/m^3 and a Moho density contrast of 400 kg/m^3. Figure 10 (bottom) shows the different Moho depth estimates along the profile. For purpose of comparison, the gravity-inverted Moho based on the combined seismic point set is shown as well. Its huge deviations from the seismic estimates again illustrate the consequences of neglecting varying crustal and mantle densities, particularly in the GSM region, where a very low density contrast of ~55 kg/m^3 at the crustal root has been modeled in order to fit both gravity and seismologically derived estimates of crustal thickness (Ferraccioli et al., 2011).

In order to examine in further detail the crustal and lithosphere properties that would be required in the thick versus thin crust scenario for the southern Wilkes Subglacial Basin, we use LitMod2D v1.6 (Afonso et al., 2008), a software that has successfully been applied in a number of studies (e.g., Jones et al., 2014). It solves the corresponding equations for conductive heat flow, thermodynamic, geopotential, and isostasy in the finite differences method simultaneously. Output data are density, temperature and pressure fields, surface heat flow, seismic body wave velocities, geoid, gravity anomalies, and isostatic elevation (topography). The underlying properties are functions of temperature, pressure, and composition. In case of mantle material, they are thermodynamically modeled with the software Perple_X (Connolly, 2005) based on a predefined peridotitic composition. Further details of the methodology are described by Afonso et al. (2008). According to the different Moho depth estimates, we set up two alternative models along the model profile (Figure 10): one with a shallow and one with a deep Moho boundary.

Petrological properties are required as input parameters for crust and mantle. We use values for bulk density, thermal expansion coefficient, and compressibility (Table 1) of the crustal layers that result in in situ densities being thought to represent a global average (e.g., Christensen & Mooney, 1995; Rudnick et al., 1998, and references therein). For thermal parameters (heat production and thermal conductivity), we take the same values as An et al. (2015b, and references therein) to get comparable results. The petrology of the upper mantle of central EANT is unknown, but it has been speculated that an igneous and metamorphic belt of Mesoproterozoic (1–1.4 Ma) age is present at crustal levels on the periphery of the GSM (Elliot et al., 2015; Ferraccioli et al., 2011; Goodge et al., 2017). Thus, we assume a mean Proterozoic lithospheric mantle composition beneath the interior of EANT in our models. However, seismic *S* wave and Rayleigh wave velocity studies beneath the 250-km-thick (An et al., 2015b) craton indicate that the lithosphere of the GSM region may have been formed during earlier Archaean and Paleoproterozoic times (Heeszel et al., 2013). Following these seismic interpretations, we introduce a lithospheric mantle of Archaean composition in our models beneath the GSM. In our modeling, we use the oxide compositions for representative Phanerozoic, Proterozoic, and Archaean peridotites from Afonso et al. (2008).

4.1. Results and Discussion

We fitted the models to topography and geoid by minor adjustments of crustal densities (see Table 1 for the parameters used and compare upper and lower table), Moho depth, and lithospheric thickness. The modeled lithospheric density structure (Figure 11, bottom) directly affects the resulting geoid and isostatic elevation, which in turn are used as constraining observables. While the model with the shallow Moho beneath the southern Wilkes Subglacial Basin could be fitted with a uniform lithospheric mantle of Proterozoic composition, the deep Moho boundary required a denser lithospheric mantle to be in isostatic balance. Overall, both the deeper and the shallower Moho scenarios can fit the topography and geoid but require different mantle compositions.

Further comparison with upper mantle *S* wave velocities (An et al., 2015a) and surface heat flow (An et al., 2015b) can be done for model validation and discussion. Remarkably different geothermal heat flow estimations exist for Antarctica (e.g., Fox Maule et al., 2005; Martos et al., 2017; Shapiro & Ritzwoller, 2004). Here

Table 1
Petrophysical Parameters of Crustal Layers in the 2-D Models

Body No.	Type	Heat prod.	Therm. cond.	Density	Compressibility
Model with deep Moho after Hansen et al. (2009)					
1a	Upper crust	1.0	2.1	2.65	6e-11
1b	Upper crust	1.0	2.1	2.80	5e-11
2a	Lower crust	0.4	2.1	2.70	6e-11
2b	Lower crust	0.5	2.2	2.80	6e-11
		($\mu W/m^3$)	(W/mK)	(g/cm^3)	(GPa^{-1})
Model with shallow Moho after Lawrence et al. (2006b)					
1a	Upper crust	1.0	2.1	2.65	6e-11
1b	Upper crust	1.0	2.1	2.78	5e-11
2a	Lower crust	0.4	2.1	2.70	6e-11
2b	Lower crust	0.3	2.2	2.78	7e-11
		($\mu W/m^3$)	(W/mK)	(g/cm^3)	(GPa^{-1})

Note. The body numbers correspond to Figure 11.

we compare our predictions to the heat flux estimates from An et al. (2015b) since they originate from a similar model setup (conductive heat transfer within the lithosphere) and are thus best suited for our 2-D modeling purposes. The calculated surface heat flow of both 2-D models (Figure 11) is in the range of heat flow data provided by An et al. (2015b). Notably, the largest effect is in the coastal region of the TAM (close to profile point A) where heat flow differs from 55 to more than 65 mW/m^2 between the two models. Such a difference would be expected to have a significant effect in modeling of the ice sheet history (e.g., Rogozhina et al., 2012) and estimates of present-day basal melting rates, which in turn can influence subglacial hydrology and ice sheet dynamics. Regarding seismic velocities, both models are in first-order

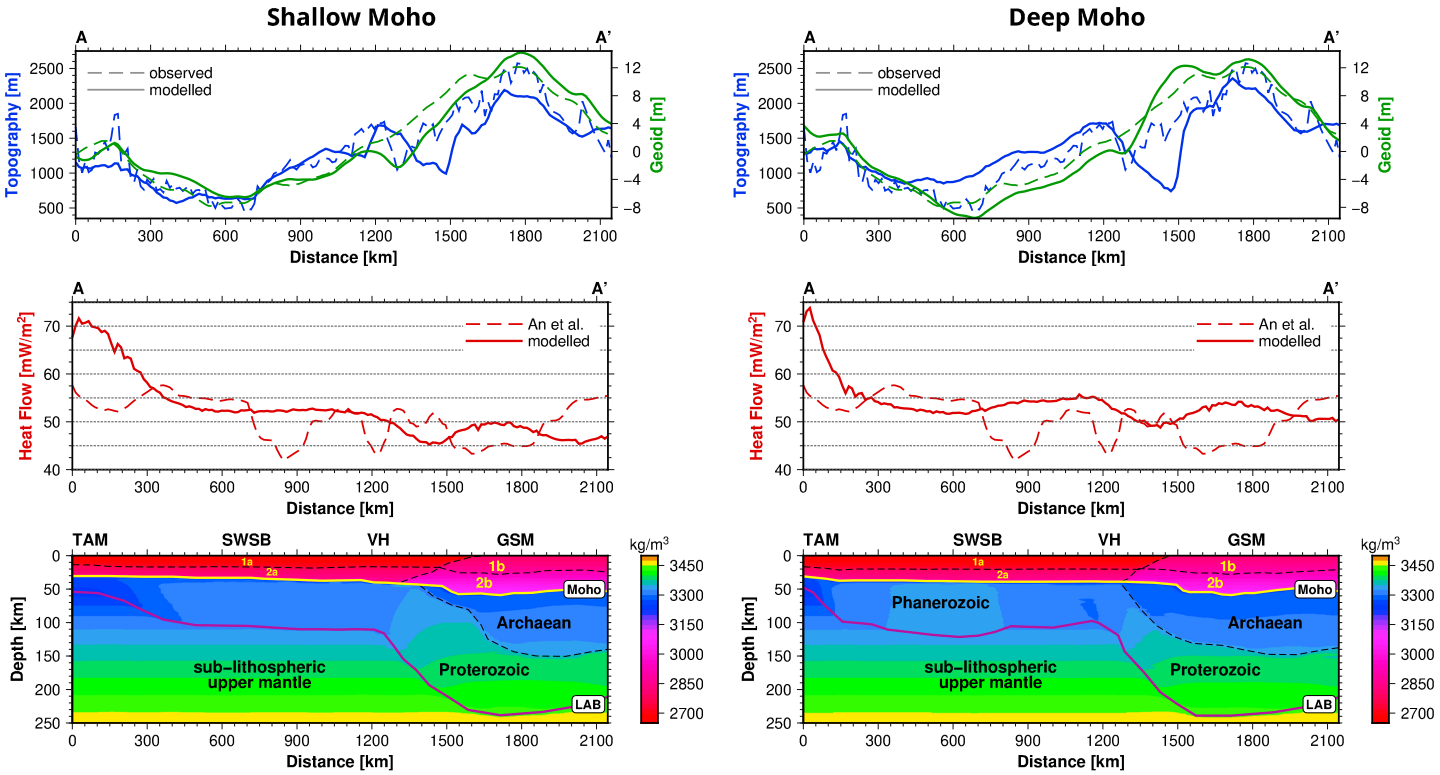

Figure 11. LitMod2D modeling results along the profile shown in Figure 10. Left: thin crust after Lawrence et al. (2006b); right: thick crust after Hansen et al. (2009). Both models are fitted for topography and geoid (top) and are largely consistent with heat flow estimations. A thick crust requires higher lithospheric mantle density to be in isostatic equilibrium. TAM = Transantarctic Mountains; SWSB = Southern Wilkes Subglacial Basin; VH = Vostok Highlands; GSM = Gamburtsev Subglacial Mountains.

agreement with the *S* wave model from An et al. (2015a) down to a depth of ~150 km (Figure 12). At profile kilometer 1,200–1,300, a transition from low to high velocities takes place at depths of 50–150 km, which is a response to the thick underlying lithosphere. However, the LitMod2D framework assumes an adiabatic temperature gradient in the sublithospheric mantle and does not include thermal anomalies there. Thus, the seismic velocities are only comparable when assuming thermal steady state. Considering that, the slightly better resemblance of the deep Moho model with the AN1 velocity model should not be considered as a robust indication of a more realistic model. The comparison of *S* wave velocities alone cannot validate or reject one of the two models, either.

A depleted mantle composition of Proterozoic age that would best fit with the thick crust scenario would be consistent with the hypothesis that the Mawson Craton of Archaean-Paleoproterozoic age that comprised the Antarctic Terre Adélie Craton and the Australian Gawler Craton prior to Gondwana breakup extends to our model profile and may extend even much further south to the Shackleton Range in Queen Elizabeth Land (Boger, 2011; Paxman et al., 2017). The notion that the Mawson Craton extends to our study area is also supported by independent observations from surface geology in the central TAM and from studies of glacial erratics. Detrital zircons from Lake Vostok, for example, are partly dated to 1.6–1.8 Ga (Leitchenkov et al., 2016) and have potentially been transported from ice sheet-covered cratonic terrains located in the Wilkes Land region. Goodge et al. (2017) collected and analyzed glacial clasts in the central TAM region, relatively close to our modeling profile. Their results indicate that ~1.6-Ga magmatic belts of the Gawler Craton may extend into central EANT. The transport distance of the individual clasts, however, is uncertain. Distinctly younger ages (ca. 1.3 to 1.0 Ga) are also observed, and their origin could be located in a putative ~1,000-km-distant source region in the GSM province, where Ferraccioli et al. (2011) hypothesized that a major coeval orogenic belt exists, based on their aeromagnetic and airborne gravity interpretation. Aeromagnetic studies also suggest that the cratonal margin of EANT, at least at crustal level, gets much closer to the coast along our modeling profile compared to the northern parts, where the Ross Orogen appears to be considerably wider (Ferraccioli, Armadillo, Jordan, et al., 2009; Ferraccioli, Armadillo, Zunino, et al., 2009; Ferraccioli et al., 2002; Golynsky et al., 2018).

As this sector of the Mawson Craton and the Ross Orogen in EANT were formerly contiguous with the Gawler Craton and the Delamerian Orogen in Australia, respectively (e.g., Finn et al., 1999), it is useful to make some first-order comparisons between these two continents in terms of crustal thickness estimates. Seismic crustal thickness estimates of 30–35 km have been derived for parts of the Delamerian Orogen in South Australia (Kennett et al., 2011; Kennett et al., 2012; Salmon et al., 2013), suggesting that this subduction-related orogenic belt did not lead to major crustal thickening. A similar setting may be envisaged in particular for the back-arc regions of the Ross Orogen that may in parts underlie the Wilkes Subglacial Basin (e.g., Ferraccioli, Armadillo, Jordan, et al., 2009; Jordan et al., 2013). However, there are complicating effects in EANT, due to the much more recent Cenozoic uplift of the TAM (at the former site of the Ross Orogen) and the associated lithospheric flexure of the craton and its margin beneath the Wilkes Subglacial Basin (e.g., Paxman et al., 2018, 2019, and references therein). Irrespectively, however, we also note that some potentially conjugate Precambrian terranes in Australia that lie along the eastern edge of the Gawler Craton appear to have anomalously thick crust, most notably the seismically defined Numil terrane that has crust up to 45 km thick close to a proposed major suture zone of inferred Paleoproterozoic or even older Archaean age (Betts et al., 2016; Curtis & Thiel, 2019). Another potentially conjugate craton region for the Wilkes Subglacial Basin basement is the Australian Curnamona Craton that is also underlain by 40- to 45-km-thick crust (Kennett et al., 2011; Kennett et al., 2012; Salmon et al., 2013). Taken together, this comparison with crustal thickness patterns observed over the much better understood Australian continent coupled with previous aeromagnetic interpretations and geological studies in this sector of EANT tends to lend more weight to the Proterozoic lithosphere model beneath the TAMSEIS seismic line.

The younger and more fertile Phanerozoic lithospheric mantle composition, which is required in the model with a deep Moho beneath the southern Wilkes Subglacial Basin, is instead apparently inconsistent with the presumed Proterozoic age of the crust (Goodge et al., 2010). However, this model cannot be ruled out either, considering the broader tectonic history of the region: the inherited TAM margin formed in the course of the late Neoproterozoic breakup of Rodinia (Elliot et al., 2015; Goodge & Finn, 2010) and extensive subduction-related metamorphism and magmatism took place during the subsequent Ross Orogeny in

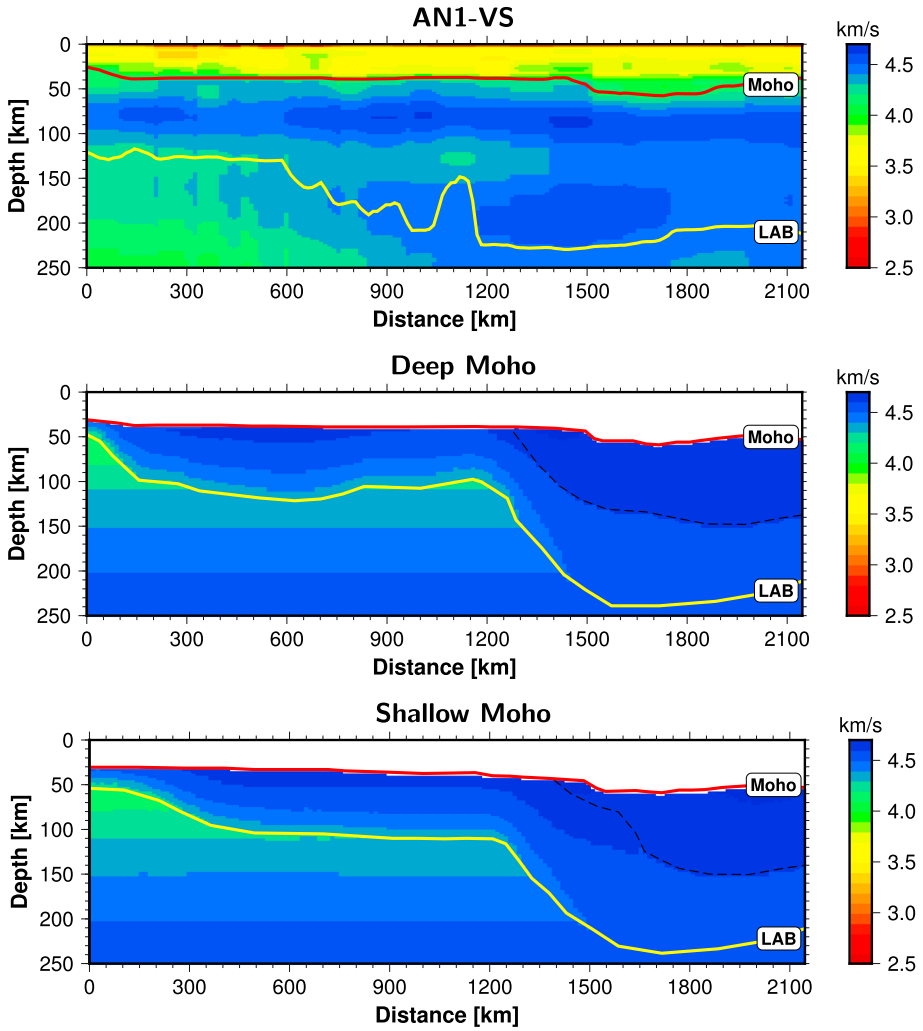

Figure 12. *S* wave velocities for the alternative models. Top: velocity model from An et al. (2015a); middle and bottom: velocities from LitMod2D models. Although the amplitude differs (partly due to the choice of attenuation parameters), the velocity pattern is widely similar down to a depth of 150 km. In the LitMod2D models only mantle velocities are calculated.

Cambrian-Ordovician times (Elliot et al., 2015; Ferraccioli, Armadillo, Jordan, et al., 2009; Ferraccioli, Armadillo, Zunino, et al., 2009; Ferraccioli et al., 2002; Ferraccioli et al., 2002, 2009; Goodge et al., 2012). Considering the above, far-field effects of Ross-age subduction in an inferred back-arc setting for the WSB region (Ferraccioli, Armadillo, Jordan, et al., 2009) could potentially have affected the degree of depletion of the mantle lithosphere beneath the hinterland of the TAM. Overall, it is possible that subduction-related processes may have led to a refertilization of the lithospheric mantle over a broader area than surface exposures or interpretations of crustal geology alone appear to support. We contend that ruling out either the thinner or the thicker crust models for the Wilkes Subglacial Basin is therefore somewhat premature based on our alternative 2-D end-member models alone. Overall, it is clear that more extensive seismological station coverage is required to reduce the ambiguities in crustal and lithospheric modeling in this remote frontier of EANT.

5. Conclusions

Our inversion results of the Moho depth of Antarctica from satellite gravity data, constrained by independent seismological estimates, are broadly consistent with previous gravity studies (Block et al., 2009; O'Donnell & Nyblade, 2014). Our main results and conclusions are summarized hereafter:

1. A strong contrast in crustal thickness is confirmed between WANT (~25 km) and the composite East Antarctic craton (~40–45 km) and the larger misfits between gravity inversions and seismologically derived estimates of Moho depth likely stem from different density contrasts at the Moho in these geologically distinct parts of the continent. A separate inversion for West and EANT therefore provides a better fit to the seismic constraints and thus yielded improved Moho depth estimates. However, we found that the different density contrasts at the Moho could not be resolved reliably from gravity inversions alone, especially beneath WANT, suggesting that there could be significant additional variability in upper mantle densities beneath the different Phanerozoic domains that make up WANT.
2. By comparing our results with an Airy-isostatic Moho depth model we showed that different modes of compensation likely exist in EANT and WANT. Notably, we found that the region of Wilkes Land also differs considerably from the rest of EANT. It is therefore reasonable to conclude that some sectors of Antarctica may not be in isostatic equilibrium and that significant additional buoyancy contributions from the lithospheric mantle are present even in EANT, in general agreement with the findings of O'Donnell and Nyblade (2014).
3. In our quest to better comprehend crustal and deeper lithospheric architecture in interior EANT, we performed targeted 2-D lithospheric modeling over the southern Wilkes Subglacial Basin region along the TAMSEIS-GAMSEIS passive seismic profile. We showed that a shallow Moho beneath the basin can be fitted by introducing a moderately depleted lithospheric mantle composition, which would match well with the notion of a Proterozoic age lithosphere underlying the region. An alternative end-member model with a deeper Moho fits the satellite gravity and the topography equally well but requires a higher mantle density, as might be expected for a younger and more fertile Phanerozoic lithospheric mantle. Although the latter model appears to be at odds with our current knowledge of this part of the Mawson Craton, based on surface geology, erratics, and interpretations of aeromagnetic anomaly data, we propose that it cannot be ruled out either. For example, far-field effects of Ross-age subduction in a distal back-arc setting (Ferraccioli et al., 2002; Ferraccioli, Armadillo, Jordan, et al., 2009) could in principle have modified the original Proterozoic lithosphere beneath parts of the Wilkes Subglacial Basin, affecting the degree of depletion of the mantle lithosphere. Given the importance of validating or refuting these competing models for the crustal structure of the Wilkes Subglacial Basin, both for comprehending the processes that affected the margin of the composite East Antarctic Craton and for geothermal heat flow estimation, we recommend new seismological deployments in this frontier region, coupled with the development of enhanced 3-D lithosphere modeling approaches.

Acknowledgments
This study was carried out in the course of the project GOCE+ Antarctica, funded by the European Space Agency ESA as a Support to Science Element. Fausto Ferraccioli acknowledges support from ESA and the Geology and Geophysics Team of the British Antarctic Survey. All grid files and maps were created using Generic Mapping Tools (GMT) version 5 (Wessel et al., 2013). The data and modeling software used are listed in the references.

References

Afonso, J. C., Fernàndez, M., Ranalli, G., Griffin, G., & Connolly, J. A. D. (2008). Integrated geophysical-petrological modeling of the lithosphere and sublithospheric upper mantle: Methodology and applications. *Geochemistry, Geophysics, Geosystems*, *9*, Q05008. https://doi.org/10.1029/2007GC001834

Aitken, A. R. A., Betts, P. G., Young, D. A., Blankenship, D. D., Roberts, J. L., & Siegert, M. J. (2016). The Australo-Antarctic Columbia to Gondwana transition. *Gondwana Research*, *29*(1), 136–152. https://doi.org/10.1016/j.gr.2014.10.019

Aitken, A. R. A., Young, D. A., Ferraccioli, F., Betts, P. G., Greenbaum, J. S., Richter, T. G., et al. (2014). The subglacial geology of Wilkes Land, East Antarctica. *Geophysical Research Letters*, *41*, 2390–2400. https://doi.org/10.1002/2014GL059405

Amante, C., & Eakins, B. W. (2009). ETOPO1 1 arc-minute global relief model: Procedures, data sources and analysis. *National Geophysical Data Center, NOAA*. https://doi.org/10.7289/V5C8276M

An, M., Wiens, D. A., Zhao, Y., Feng, M., Nyblade, A., Kanao, M., et al. (2015b). Temperature, lithosphere–asthenosphere boundary, and heat flux beneath the Antarctic Plate inferred from seismic velocities. *Journal of Geophysical Research: Solid Earth.*, *120*, 8720–8742. https://doi.org/10.1002/2015JB011917

An, M., Wiens, D. A., Zhao, Y., Feng, M., Nyblade, A. A., Kanao, M., et al. (2015a). S-velocity model and inferred Moho topography beneath the Antarctic Plate from Rayleigh waves. *Journal of Geophysical Research: Solid Earth*, *120*, 359–383. https://doi.org/10.1002/2014JB011332

Baranov, A., & Morelli, A. (2013). The Moho depth map of the Antarctica region. *Tectonophysics*, *609*, 299–313. https://doi.org/10.1016/j.tecto.2012.12.023

Betts, P. G., Armit, R. J., Stewart, J., Aitken, A. R. A., Ailleres, L., Donchak, P., et al. (2016). Australia and Nuna. *Geological Society, London, Special Publications*, *424*(1), 47–81. https://doi.org/10.1144/SP424.2

Block, A. E., Bell, R. E., & Studinger, M. (2009). Antarctic crustal thickness from satellite gravity: Implications for the Transantarctic and Gamburtsev Subglacial Mountains. *Earth and Planetary Science Letters*, *288*(1–2), 194–203. https://doi.org/10.1016/j.epsl.2009.09.022

Boger, S. D. (2011). Antarctica—Before and after Gondwana. *Gondwana Research*, *19*(2), 335–371. https://doi.org/10.1016/j.gr.2010.09.003

Chaput, J., Aster, R. C., Huerta, A., Sun, X., Lloyd, A., Wiens, D., & Wilson, T. (2014). The crustal thickness of West Antarctica. *Journal of Geophysical Research: Solid Earth*, *119*, 378–395. https://doi.org/10.1002/2013JB010642

Chiappini, M., Ferraccioli, F., Bozzo, E., & Damaske, D. (2002). Regional compilation and analysis of aeromagnetic anomalies for the Transantarctic Mountains-Ross Sea sector of the Antarctic. *Tectonophysics*, *347*(1-3), 121–137. https://doi.org/10.1016/S0040-1951(01)00241-4

Christensen, N. I., & Mooney, W. D. (1995). Seismic velocity structure and composition of the continental crust: A global view. *Journal of Geophysical Research*, *100*(B6), 9761–9788. https://doi.org/10.1029/95JB00259

Collins, A. S., & Pisarevsky, S. A. (2005). Amalgamating eastern Gondwana: The evolution of the Circum-Indian Orogens. *Earth-Science Reviews*, *71*(3–4), 229–270. https://dx.doi.org/10.1016/j.earscirev.2005.02.004

Connolly, J. A. (2005). Computation of phase equilibria by linear programming: A tool for geodynamic modeling and its application to subduction zone decarbonation. *Earth and Planetary Science Letters*, *236*(1–2), 524–541. https://doi.org/10.1016/j.epsl.2005.04.033

Creyts, T. T., Ferraccioli, F., Bell, R. E., Wolovick, M., Corr, H., Rose, K. C., et al. (2014). Freezing of ridges and water networks preserves the Gamburtsev Subglacial Mountains for millions of years. *Geophysical Research Letters*, *41*, 8114–8122. https://doi.org/10.1002/2014GL061491

Curtis, S., & Thiel, S. (2019). Identifying lithospheric boundaries using magnetotellurics and Nd isotope geochemistry: An example from the Gawler Craton, Australia. *Precambrian Research*, *320*, 403–423. https://doi.org/10.1016/j.precamres.2018.11.013

Ebbing, J., Haas, P., Ferraccioli, F., Pappa, F., Szwillus, W., & Bouman, J. (2018). Earth tectonics as seen by GOCE—Enhanced satellite gravity gradient imaging. *Scientific Reports*, *8*(1), 16356. https://doi.org/10.1038/s41598-018-34733-9

Elliot, D. H., Fanning, C. M., & Hulett, S. R. W. (2015). Age provinces in the Antarctic craton: Evidence from detrital zircons in Permian strata from the Beardmore Glacier region, Antarctica. *Gondwana Research*, *28*(1), 152–164. https://doi.org/10.1016/j.gr.2014.03.013

Ferraccioli, F., Armadillo, E., Jordan, T., Bozzo, E., & Corr, H. (2009). Aeromagnetic exploration over the East Antarctic Ice Sheet: A new view of the Wilkes Subglacial Basin. *Tectonophysics*, *478*(1–2), 62–77. https://doi.org/10.1016/j.tecto.2009.03.013

Ferraccioli, F., Armadillo, E., Zunino, A., Bozzo, E., Rocchi, S., & Armienti, P. (2009). Magmatic and tectonic patterns over the Northern Victoria Land sector of the Transantarctic Mountains from new aeromagnetic imaging. *Tectonophysics*, *478*(1-2), 43–61. https://doi.org/10.1016/j.tecto.2008.11.028

Ferraccioli, F., & Bozzo, E. (2003). Cenozoic strike-slip faulting from the eastern margin of the Wilkes Subglacial Basin to the western margin of the Ross Sea Rift: An aeromagnetic connection. *Geological Society, London, Special Publications*, *210*(1), 109–133. https://doi.org/10.1144/GSL.SP.2003.210.01.07

Ferraccioli, F., Bozzo, E., & Capponi, G. (2002). Aeromagnetic and gravity anomaly constraints for an early Paleozoic subduction system of Victoria Land, Antarctica. *Geophysical Research Letters*, *29*(10), 1406. https://doi.org/10.1029/2001GL014138

Ferraccioli, F., Coren, F., Bozzo, E., Zanolla, C., Gandolfi, S., Tabacco, I., & Frezzotti, M. (2001). Rifted(?) crust at the East Antarctic Craton margin: Gravity and magnetic interpretation along a traverse across the Wilkes Subglacial Basin region. *Earth and Planetary Science Letters*, *192*(3), 407–421. https://doi.org/10.1016/S0012-821X(01)00459-9

Ferraccioli, F., Finn, C. A., Jordan, T. A., Bell, R. E., Anderson, L. M., & Damaske, D. (2011). East Antarctic rifting triggers uplift of the Gamburtsev Mountains. *Nature*, *479*(7373), 388–392. https://doi.org/10.1038/nature10566

Finn, C., Moore, D., Damaske, D., & Mackey, T. (1999). Aeromagnetic legacy of early Paleozoic subduction along the Pacific margin of Gondwana. *Geology*, *27*(12), 1087–1090. https://doi.org/10.1130/0091-7613(1999)027%3C1087:ALOEPS%3E2.3.CO;2

Fox Maule, C., Purucker, M. E., Olsen, N., & Mosegaard, K. (2005). Heat flux anomalies in Antarctica revealed by satellite magnetic data. *Science*, *309*(5733), 464–467. https://doi.org/10.1126/science.1106888

Fretwell, P., Pritchard, H. D., Vaughan, D. G., Bamber, J. L., Barrand, N. E., Bell, R., et al. (2013). Bedmap2: Improved ice bed, surface and thickness datasets for Antarctica. https://doi.org/10.5194/tc-7-375-2013

Fullea, J., Afonso, J. C., Connolly, J. A. D., Fernàndez, M., Garcìa-Castellanos, D., & Zeyen, H. (2009). LitMod3D: An interactive 3-D software to model the thermal, compositional, density, rheological and seismological structure of the lithosphere and sublithospheric upper mantle. *Geochemistry, Geophysics, Geosystems*, *10*, Q08019. https://doi.org/10.1029/2009GC002391

Golynsky, A., Chiappini, M., Damaske, D., Ferraccioli, F., Finn, C. A., Ishihara, T., et al. (2006). ADMAP — A digital magnetic anomaly map of the Antarctic. In D. K. Fütterer, D. Damaske, G. Kleinschmidt, H. Miller, & F. Tessensohn (Eds.), *Antarctica: Contributions to global earth sciences* (pp. 109–116). Berlin, Heidelberg: Springer Berlin Heidelberg. https://doi.org/10.1007/3-540-32934-X_12

Golynsky, A. V., Ferraccioli, F., Hong, J. K., Golynsky, D. A., von Frese, R. R. B., Young, D. A., et al. (2018). New magnetic anomaly map of the Antarctic. *Geophysical Research Letters*, *45*, 6437–6449. https://doi.org/10.1029/2018GL078153

Goodge, J. W., Fanning, C. M., Brecke, D. M., Licht, K. J., & Palmer, E. F. (2010). Continuation of the Laurentian Grenville Province across the Ross Sea margin of East Antarctica. *The Journal of Geology*, *118*(6), 601–619. https://doi.org/10.1086/656385

Goodge, J. W., Fanning, C. M., Fisher, C. M., & Vervoort, J. D. (2017). Proterozoic crustal evolution of central East Antarctica: Age and isotopic evidence from glacial igneous clasts, and links with Australia and Laurentia. *Precambrian Research*, *299*, 151–176. https://doi.org/10.1016/j.precamres.2017.07.026

Goodge, J. W., Fanning, C. M., Norman, M. D., & Bennett, V. C. (2012). Temporal, isotopic and spatial relations of early Paleozoic Gondwana-margin arc magmatism, central Transantarctic Mountains, Antarctica. *Journal of Petrology*, *53*(10), 2027–2065. https://doi.org/10.1093/petrology/egs043

Goodge, J. W., & Finn, C. A. (2010). Glimpses of East Antarctica: Aeromagnetic and satellite magnetic view from the central Transantarctic Mountains of East Antarctica. *Journal of Geophysical Research*, *115*, B09103. https://doi.org/10.1029/2009JB006890

Hansen, S. E., Graw, J. H., Kenyon, L. M., Nyblade, A. A., Wiens, D. A., Aster, R. C., et al. (2014). Imaging the Antarctic mantle using adaptively parameterized P-wave tomography: Evidence for heterogeneous structure beneath West Antarctica. *Earth and Planetary Science Letters*, *408*, 66–78. https://doi.org/10.1016/j.epsl.2014.09.043

Hansen, S. E., Julià, J., Nyblade, A. A., Pyle, M. L., Wiens, D. A., & Anandakrishnan, S. (2009). Using S wave receiver functions to estimate crustal structure beneath ice sheets: An application to the Transantarctic Mountains and East Antarctic craton. *Geochemistry, Geophysics, Geosystems*, *10*, Q08014. https://doi.org/10.1029/2009GC002576

Hansen, S. E., Nyblade, A. A., Heeszel, D. S., Wiens, D. A., Shore, P., & Kanao, M. (2010). Crustal structure of the Gamburtsev Mountains, East Antarctica, from S-wave receiver functions and Rayleigh wave phase velocities. *Earth and Planetary Science Letters*, *300*(3–4), 395–401. https://doi.org/10.1016/j.epsl.2010.10.022

Heeszel, D. S., Wiens, D. A., Nyblade, A. A., Hansen, S. E., Kanao, M., An, M., & Zhao, Y. (2013). Rayleigh wave constraints on the structure and tectonic history of the Gamburtsev Subglacial Mountains, East Antarctica. *Journal of Geophysical Research: Solid Earth*, *118*, 2138–2153. https://doi.org/10.1002/jgrb.50171

Jones, A. G., Afonso, J. C., Fullea, J., & Salajegheh, F. (2014). The lithosphere-asthenosphere system beneath Ireland from integrated geophysical-petrological modeling—I: Observations, 1D and 2D hypothesis testing and modeling. *Lithos*, *189*, 28–48. https://doi.org/10.1016/j.lithos.2013.10.033

Jordan, T. A., Ferraccioli, F., Armadillo, E., & Bozzo, E. (2013). Crustal architecture of the Wilkes Subglacial Basin in East Antarctica, as revealed from airborne gravity data. *Tectonophysics*, *585*, 196–206. https://doi.org/10.1016/j.tecto.2012.06.041

Kanao, M., Wiens, D., Tanaka, S., Nyblade, A., Toyokuni, G., Shore, P., et al. (2014). Broadband seismic deployments in East Antarctica: IPY contribution to monitoring the Earth's interiors. *Annals of Geophysics*, *57*(3). https://doi.org/10.4401/ag-6379

Kennett, B. L. N., Salmon, M., Saygin, E., & Group, A. W. (2011). AusMoho: The variation of Moho depth in Australia. *Geophysical Journal International*, *187*(2), 946–958. https://doi.org/10.1111/j.1365-246X.2011.05194.x

Kennett, B. L. N., Saygin, E., & Salmon, M. (2012). Australian Seismological Reference Model (AuSREM): Crustal component. *Geophysical Journal International*, *192*(1), 190–206. https://doi.org/10.1093/gji/ggs004

Lawrence, J. F., Wiens, D. A., Nyblade, A. A., Anandakrishnan, S., Shore, P. J., & Voigt, D. (2006a). Crust and upper mantle structure of the Transantarctic Mountains and surrounding regions from receiver functions, surface waves, and gravity: Implications for uplift models. *Geochemistry, Geophysics, Geosystems*, *7*, Q10011. https://doi.org/10.1029/2006GC001282

Lawrence, J. F., Wiens, D. A., Nyblade, A. A., Anandakrishnan, S., Shore, P. J., & Voigt, D. (2006b). Rayleigh wave phase velocity analysis of the Ross Sea, Transantarctic Mountains, and East Antarctica from a temporary seismograph array. *Journal of Geophysical Research*, *111*, B06302. https://doi.org/10.1029/2005JB003812

Leitchenkov, G. L., Antonov, A. V., Luneov, P. I., & Lipenkov, V. Y. (2016). Geology and environments of subglacial Lake Vostok. *Philosophical Transactions of the Royal Society A: Mathematical, Physical and Engineering Sciences*, *374*(2059), 20140302. https://doi.org/10.1098/rsta.2014.0302

Li, X., & Götze, H.-J. (2001). Ellipsoid, geoid, gravity, geodesy, and geophysics. *Geophysics*, *66*(6), 1660–1668. https://doi.org/10.1190/1.1487109

Martos, Y. M., Catalán, M., Jordan, T. A., Golynsky, A., Golynsky, D., Eagles, G., & Vaughan, D. G. (2017). Heat flux distribution of Antarctica unveiled. *Geophysical Research Letters*, *44*, 11,417–11,426. https://doi.org/10.1002/2017GL075609

Mayer-Guerr, T. (2015). The combined satellite gravity field model GOCO05s. In EGU General Assembly Conference Abstracts (Vol. 17, p. 12,364).

O'Donnell, J. P., & Nyblade, A. A. (2014). Antarctica's hypsometry and crustal thickness: Implications for the origin of anomalous topography in East Antarctica. *Earth and Planetary Science Letters*, *388*, 143–155. https://doi.org/10.1016/j.epsl.2013.11.051

Paxman, G. J. G., Jamieson, S. S. R., Ferraccioli, F., Bentley, M. J., Forsberg, R., Ross, N., et al. (2017). Uplift and tilting of the Shackleton Range in East Antarctica driven by glacial erosion and normal faulting. *Journal of Geophysical Research: Solid Earth.*, *122*, 2390–2408. https://doi.org/10.1002/2016JB013841

Paxman, G. J. G., Jamieson, S. S. R., Ferraccioli, F., Bentley, M. J., Ross, N., Armadillo, E., et al. (2018). Bedrock erosion surfaces record former East Antarctic ice sheet extent. *Geophysical Research Letters*, *45*, 4114–4123. https://doi.org/10.1029/2018GL077268

Paxman, G. J. G., Jamieson, S. S. R., Ferraccioli, F., Bentley, M. J., Ross, N., Watts, A. B., et al. (2019). The role of lithospheric flexure in the landscape evolution of the Wilkes Subglacial Basin and Transantarctic Mountains, East Antarctica. *Journal of Geophysical Research: Earth Surface*. https://doi.org/10.1029/2018JF004705

Paxman, G. J. G., Watts, A. B., Ferraccioli, F., Jordan, T. A., Bell, R. E., Jamieson, S. S. R., & Finn, C. A. (2016). Erosion-driven uplift in the Gamburtsev Subglacial Mountains of East Antarctica. *Earth and Planetary Science Letters*, *452*, 1–14. https://doi.org/10.1016/j.epsl.2016.07.040

Ramirez, C., Nyblade, A., Emry, E., Julià, J., Sun, X., Anandakrishnan, S., et al. (2017). Crustal structure of the Transantarctic Mountains, Ellsworth Mountains and Marie Byrd Land, Antarctica: Constraints on shear wave velocities, Poisson's ratios and Moho depths. *Geophysical Journal International* Retrieved from, *211*(3), 1328–1340. https://doi.org/10.1093/gji/ggx333

Ramirez, C., Nyblade, A., Hansen, S. E., Wiens, D. A., Anandakrishnan, S., Aster, R. C., et al. (2016). Crustal and upper-mantle structure beneath ice-covered regions in Antarctica from S-wave receiver functions and implications for heat flow. *Geophysical Journal International*, *204*(3), 1636–1648. https://doi.org/10.1093/gji/ggv542

Rogozhina, I., Hagedoorn, J. M., Martinec, Z., Fleming, K., Soucek, O., Greve, R., & Thomas, M. (2012). Effects of uncertainties in the geothermal heat flux distribution on the Greenland ice sheet: An assessment of existing heat flow models. *Journal of Geophysical Research*, *117*, F02025. https://doi.org/10.1029/2011JF002098

Rudnick, R. L., McDonough, W. F., & O'Connell, R. J. (1998). Thermal structure, thickness and composition of continental lithosphere. *Chemical Geology*, *145*(3–4), 395–411. https://doi.org/10.1016/S0009-2541(97)00151-4

Salmon, M., Kennett, B. L. N., Stern, T., & Aitken, A. R. A. (2013). The Moho in Australia and New Zealand. *Tectonophysics*, *609*, 288–298. https://doi.org/10.1016/j.tecto.2012.07.009

Scheinert, M., Ferraccioli, F., Schwabe, J., Bell, R., Studinger, M., Damaske, D., et al. (2016). New Antarctic gravity anomaly grid for enhanced geodetic and geophysical studies in Antarctica. *Geophysical Research Letters*, *43*, 600–610. https://doi.org/10.1002/2015GL067439

Sebera, J., Haagmans, R., Floberghagen, R., & Ebbing, J. (2018). Gravity spectra from the density distribution of Earth's uppermost 435 km. *Surveys in Geophysics*, *39*(2), 227–244. https://doi.org/10.1007/s10712-017-9445-z

Sebera, J., Šprlák, M., Novák, P., Bezděk, A., & Vaľko, M. (2014). Iterative spherical downward continuation applied to magnetic and gravitational data from satellite. *Surveys in Geophysics*, *35*(4), 941–958. https://doi.org/10.1007/s10712-014-9285-z

Shapiro, N. M., & Ritzwoller, M. H. (2004). Inferring surface heat flux distributions guided by a global seismic model: Particular application to Antarctica. *Earth and Planetary Science Letters*, *223*(1–2), 213–224. https://doi.org/10.1016/j.epsl.2004.04.011

Shen, W., Wiens, D. A., Anandakrishnan, S., Aster, R. C., Gerstoft, P., Bromirski, P. D., et al. (2018). The crust and upper mantle structure of central and West Antarctica from Bayesian inversion of Rayleigh wave and receiver functions. *Journal of Geophysical Research: Solid Earth*, *123*(9), 7824–7849. https://doi.org/10.1029/2017JB015346

Shen, W., Wiens, D. A., Stern, T., Anandakrishnan, S., Aster, R. C., Dalziel, I., et al. (2017). Seismic evidence for lithospheric foundering beneath the southern Transantarctic Mountains, Antarctica. *Geology*, *46*(1), 71–74. https://doi.org/10.1130/G39555.1

Studinger, M., Bell, R. E., Buck, W. R., Karner, G. D., & Blankenship, D. D. (2004). Sub-ice geology inland of the Transantarctic Mountains in light of new aerogeophysical data. *Earth and Planetary Science Letters*, *220*(3–4), 391–408. https://doi.org/10.1016/S0012-821X(04)00066-4

Szwillus, W., Ebbing, J., & Holzrichter, N. (2016). Importance of far-field topographic and isostatic corrections for regional density modeling. *Geophysical Journal International*, *207*(1), 274–287. https://doi.org/10.1093/gji/ggw270

Uieda, L., & Barbosa, V. C. F. (2017). Fast nonlinear gravity inversion in spherical coordinates with application to the South American Moho. *Geophysical Journal International*, *208*(1), 162–176. https://doi.org/10.1093/gji/ggw390

Wessel, P., Smith, W. H. F., Scharroo, R., Luis, J., & Wobbe, F. (2013). Generic mapping tools: Improved version released. *Eos, Transactions of the American Geophysical Union*, *94*(45), 409–410. https://doi.org/10.1002/2013EO450001